Turkish Online Journal of Qualitative Inquiry (TOJQI)
Volume 12, Issue 6, July 2021: 9065-9083

Research Article

Delta-Bar-Delta Neural Network (NN) Control of Voltage Source Converter Based Adaptive Control Scheme for Power Quality Improved Grid-Interactive Solar PV-Battery System

Dr.N.C. Kotaiah [1], G. Veeranjaneyulu [2], Y. Sumanth [3], Y. Mallikharjuna Rao [4],
B. Sarath Chandra [5], V. Sarayu [6]

Abstract

This paper present grid interaction solar PV-battery systems can handle unbalanced and balanced three-phase four-wire (3P-4W) nonlinear loads as well as single-phase loads of various types. AL-BP control is capable of automatically adjusting complex nonlinear systems including grid-interactive 3-phase, 4-wire systems that have critical imbalance, and feeding highly nonlinear loads, without requiring any additional tuning. A robust control mechanism is needed to improve performance of the system and power quality for solar array solar energy conversion systems. The module neural network management incorporates DSTATCOM functions such as minimizing harmonics, balancing of load, and improving power factor. The fuzzy logic control technique delivers superior precision due to the neural network's combinational neural structure. This validation validates that the system is capable of maintaining power quality, according to IEEE-519 requirements. This type of approach significantly increases the steady-state and dynamic capabilities of a grid-connected 3-phase, 4-wire (3P-4W) PV-battery system. For verification, a real-time DSP processor has been used to implement the AL-BP control technique.

Keywords: *Solar photovoltaic, Delta-Bar-Delta Neural network, four-legged IGBT-based voltage source converter, Power quality, Non-Linear loads, Integrated System, Point of common connection.*

[1] Professor, R.V.R & J.C College of Engineering (nckotaiah@rvrjc.ac.in)
[2] Asst.Professor, R.V.R & J.C College of Engineering (gvanjaneyulu@rvrjc.ac.in)
[3] Asst.Professor, R.V.R & J.C College of Engineering (sumanth46@gmail.com)
[4] Asst.Professor, R.V.R & J.C College of Engineering (ymallieee@gmail.com)
[5] Asst.Professor, R.V.R & J.C College of Engineering (sarath.boppudi@gmail.com)
[6] Asst.Professor, R.V.R & J.C College of Engineering (sarayu.vunnam@gmail.com)

I. INTRODUCTİON

Environmental concerns, technical advances, and price reductions have led to considerable growth in solar-photovoltaic (PV) powered power generation in the last few years. Greenhouse gas emissions produced by thermal power plants are substantial. Due to the availability of renewable energy, solar-photovoltaic power plants have shown to be more suitable and superior to conventional electrical power generation methods. The pertaining to one's geographical position While adaptive control systems are more suitable for linear systems or other non-linear systems, [1] shows that adaptive control systems with self-tuning capabilities may benefit even those types of systems. Neural network methods are often used in nonlinear adaptive filtering systems. This investigation consisted of using an adaptive artificial neural network for electrical utility systems for a transient stability assessment [3]. the back propagation neural network-based training technique is discussed in this article. Back propagation through time base learning is another adaptive control technique that has been previously discussed in [5]. [6] presents a back propagation neutral network for compensating in optical current sensors that use photonic transducers. For example, a multi-layer neutral network system's adaptive output tracking architecture is used to train nonlinear plants. Power market dynamic transfer capacity may be assessed using a wavelet neural network. It is feasible to approximate the error using a basic back-propagation neural network [9]. A nonlinear adaptive neural network that controls multivariable motion systems was addressed in [10]. To explain in more detail, we have explained in [11] a neural network adaptive back propagation learning technique in the following table. A neurofuzzy system used to mimic a switching reluctance motor proved very adaptable. A hybrid learning system that is both efficient and effective has been created by combining linear least squares estimation methods with a back propagation algorithm. In [13] several adaptive neutral networks for control systems have been developed. A neutral network of efficient neutral algorithms is proposed in [14] to build an auto-reclosing system. A control technique for synchronous generators has been developed in the form of a direct adaptive neutral-based method, proposed in [15]. Resonator bank structure control has been explained in [16] using a technique using back propagation neural networks. Also, the technique proposed in the citation, [17], offers an optimum adaptive learning algorithm for error-back propagation networks. Three phase four wire shunt and series active filter controls are used in an unbalanced system with [18] as the reference system. Ryan et al. [19] propose a three-phase, four-wire inverter and controller for unbalanced systems using the unique decoupling quad

transformation matrix they have used. A novel multifunctional three-phase, four-wire grid-connected compensator was described in this paper. Zeng et al. propose a modular multifunctional distributed generating unit that utilizes a 3H bridge converter for low voltage systems. The final results show an adaptive fuzzy logic and hysteresis controller that uses a three-phase, four-wire full bridge interleaved buck active power filter for high power applications. The decentralized control method proposed by Karimi et al. [23-24] is recommended for power management and load sharing in island microgrids. A control algorithm for a microgrid based on solar, wind, and battery energy storage devices was developed by Merabet et al. [25] for a standalone microgrid. A photovoltaic battery-powered fast electric vehicle charging station (station) uses a flow of electricity that maximizes the amount of electricity that gets delivered. As a consequence, solar PV, battery-assisted systems' power quality may be improved. The power quality system presented delivers extremely non-sinusoidal currents to nonlinear and unbalanced loads, such as industrial and residential loads in single- and three-phase. For verification, a real-time DSP processor has been used to implement the AL-BP control technique.

II. SCHEME AND WORKING PRINCIPLE

In Fig. 1, you can see the block diagram of the proposed improved power quality, which includes the use of sophisticated AL-BP control. (a). The recommended system operates in three-phase balanced mode while handling high-unbalanced and nonlinear loads. A four-legged IGBT-based voltage source converter (VSC) has three inductors that connect between the grid and VSC, and is further made up of a solar-PV array, a buck converter for MPPT, a 3-phase RC filter, a storage battery, a DC bus capacitor, and a bidirectional DC-DC converter for battery charging. A VSC linked to the AC grid should have an inductor that is connected to the neutrals (source and load) both. The fourth leg of VSC supplies all the harmonics needed by the negative of the load. Based on these findings, it is concluded that electricity on the neutral line is not needed. To meet design specifications, a DSP-based controller is used to produce eight gating pulses for the four leg dc voltage converter's IGBT switches from the eight applied control voltages, and those eight gating pulses are distributed among the four IGBT switches to produce the required number of switching pulses. VSC is controlled due to the use of the adaptive learning approach and back-propagation control mechanism. Incremental conductance (the incremental conductance method in this instance) is used to keep power tracking in the recommended range [30-31]. A bidirectional converter aids the

charging and discharging of batteries. Reactive power is supplied to the VSC to maintain a steady system voltage at the point of common connection (PCC). By providing almost unity power factor and correcting both reactive and harmonic currents needed by the load, it enhances system power quality.

III. CONTROL ALGORITHM

Control method for AL-BP modeling is shown in the table below. For that reason, the common-coupling voltage is expected to be,

$$V_t = \sqrt{\frac{2}{3} \times \left(V_{gaR}^2 + V_{gbY}^2 + V_{gcB}^2\right)} \quad (1)$$

In-phase normalized signal of grid voltages are estimated as follows,

$$u_{Ra} = \frac{V_{gaR}}{V_t} \quad u_{Yb} = \frac{V_{gbY}}{V_t} \quad u_{Bc} = \frac{V_{gcB}}{V_t} \quad (2)$$

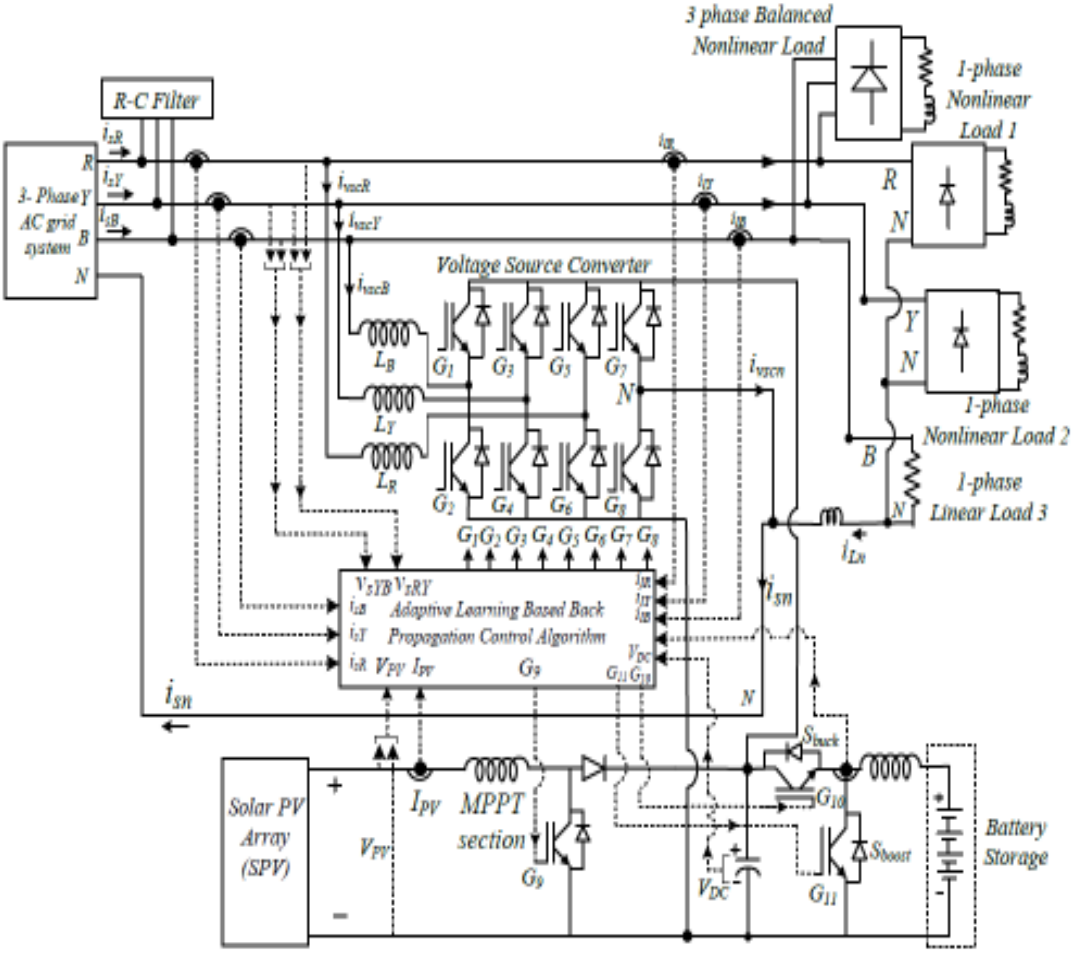

Figure 1. Block diagram of adaptive control of voltege source converter for grid-interactive solar PV-battery system feeding unbalanced 3 phase and single phase non linear loads

For the phase voltages of the grid, there are three options: VRR, VYR, and VB (also known as VRB). signals computed in the following manner: They are adjusted by quadrature of grid voltage values.

$$u_{R\alpha} = \frac{-u_{Yp} + u_{Bp}}{\sqrt{3}} \quad u_{Y\beta} = \frac{3u_{Rp} + u_{Yp} - u_{Bp}}{2\sqrt{3}}$$

$$u_{R\beta} = \frac{3u_{Rp} + u_{Yp} \quad u_{Bp}}{2\sqrt{3}} \qquad (3)$$

AL-BP control method uses equations (4) and (5) to determine the weight of the active and reactive load currents (15). Hall Effect sensors detect ilR, ily, and ilb and every sample interval is sent to the DSP controller with these values (as input variables). procedures (6) and (7). (6).

$$I_{lRp} = W_m + i_{lR}u_{Rp} + i_{lR}u_{Yp} + i_{lR}u_{Bp} \qquad (4)$$

$$I_{lYp} = W_m + i_{lY}u_{Rp} + i_{lY}u_{Yp} + i_{lY}u_{Bp} \qquad (5)$$

$$I_{lBp} = W_m + i_{lB}u_{Rp} + i_{lB}u_{Yp} + i_{lB}u_{Bp} \qquad (6)$$

Wm. the weight of the original An activation function sigmoid-type is used to the computation of fundamental load currents such as IlRp, IlYp, and IlBp (9). The results of the feed-forward block must be estimated using these equations.

$$Z_{Rp} = f(i_{lRp}) = \left(\frac{1}{1+e^{-i_{lRp}}}\right) \qquad (7)$$

$$Z_{Yp} = f(i_{lYp}) = \left(\frac{1}{1+e^{-i_{lYp}}}\right) \qquad (8)$$

$$Z_{Bp} = f(i_{lBp}) = \left(\frac{1}{1+e^{-i_{lBp}}}\right) \qquad (9)$$

(hidden in a back - propagation algorithm are ZRp, ZYp, and ZBp) (RPNN). the outputs of the hidden layer are estimated using Equations (10) and (11). (12).

$$i_{Rpl} = W_{ml} + W_{Rp}Z_{Rp} + W_{Yp}Z_{Rp} + W_{Bp}Z_{Rp} \qquad (10)$$

$$i_{Ypl} = W_{ml} + W_{Rp}Z_{Yp} + W_{Yp}Z_{Yp} + W_{Bp}Z_{Yp} \qquad (11)$$

$$i_{Bpl} = W_{ml} + W_{Rp}Z_{Bp} + W_{Yp}Z_{Bp} + W_{Bp}Z_{Bp} \qquad (12)$$

These are the initial-weights of the hidden-layer (Wm1, WRp, WYp, WBp).

$$W_{Rp}(k) = W_p(k) + \eta\left[W_p(k) - W_{Rp1}(k)\right]/i_{Rpl}\left]Z_{Rp}(k)\right. \qquad (13)$$

During the kth sample period, the active power component of load currents weighs Wp(k) and the phase R in load current calculation weighs WRp(k). This is the average value of the

active power (power going into the component itself) in phase R of the active R power flows and the feed-forward block output at the kth sampling period. iRp1 (f (iRp1). A constant is used to calculate the learning rate of a proposed neural network-based control system. an algebraic equation (14) (15). (15),

$$W_{Rp}(k)=W_{p}(k)+\eta\left[W_{p}(k)-W_{Rp1}(k)\right]f'\left(i_{Rp1}\right)Z_{Rp}(k) \quad (14)$$

$$W_{Bp}(k)=W_{p}(k)+\eta\left[W_{p}(k)-W_{Bp1}(k)\right]f'\left(i_{Bp1}\right)Z_{Bp}(k) \quad (15)$$

The numerical parameters of iRp1, iYp1, and iBp1 are processed by the neural network's activation function.

$$W_{Rp1}=f\left(i_{iRp1}\right)=\left(\frac{1}{1+e^{-i_{Rp1}}}\right) \quad (16)$$

$$W_{Yp1}=f\left(i_{iYp1}\right)=\left(\frac{1}{1+e^{-i_{Yp1}}}\right) \quad (17)$$

$$W_{Bp1}=f\left(i_{iBp1}\right)=\left(\frac{1}{1+e^{-i_{Bp1}}}\right) \quad (18)$$

Here's how to compute average weight of basic real power signal

$$Z_{Rp}=f\left(i_{iRp}\right)=\left(\frac{1}{1+e^{-i_{Rp}}}\right) \quad (19)$$

Following the low pass filter, a scaling factor (ξ) is used to get the final weight of the real power component Wlpt. The actual cost of imaginary power component is calculated by multiplying the base values by the scaling factor (). (Wlqt). Bidirectional DC-DC power converter can be seen in Figure 2. Battery storage systems are one of the primary uses of this product (BES). The nominal voltage of the BES is maintained while it is charging. The PI controllers utilize input Sensored DC link voltage and reference DC link voltage. The reference battery current is detected, and the PI controller output is compared to it to calculate the bidirectional DC-DC converter BES current. It is anticipated that the overall DC link voltage error will be

$$V_{dcE}(k)=V_{dc}^{*}(k)-V_{dc}(k) \quad (20)$$

The output of this PI controller is as follows.

$$I_{PL}(k)=I_{PL}(k-1)+K_{if}\left\{V_{dcE}(k)-V_{dcE}(k-1)\right\}+K_{pf}V_{dcE}(k) \quad (21)$$

These gain parameters for the PI controller in the DC link voltage control loop are kpf and kif. For actual grid current ($W_{Y}p$), the power contribution is:

$$W_{Yp1}=f\left(i_{iYp1}\right)=\left(\frac{1}{1+e^{-i_{Yp1}}}\right) \quad (22)$$

To achieve DC link voltage control in the DC link voltage control, the PI controller's gain constants are set to kpf and kif. For actual grid current (W_Bp), the power contribution is:

$$W_{Bp1} = f(i_{1Bp1}) = \left(\frac{1}{1+e^{-i_{Bp1}}}\right) \quad (23)$$

Its production is as follows.

$$V(k) = \tilde{V}(k-1) + K_{in}\{V_{TE}(k) - V_{TE}(k-1)\} + K_{pn}V_{TE}(k) \quad (24)$$

(WFq) is computed as a function of the imaginary power component of the grid currents.

follows, $V_{dc\,E}(k) = V_{dc}^{*}(k) - V_{dc}(k)$ (25)

These are the actual components of reference grid currents.

$$i_{sRp} = W_{Fp}u_{Rp},\ i_{sYp} = W_{Fp}u_{Yp},\ i_{sBp} = W_{Fp}u_{Bp} \quad (26)$$

These are the reactive components of grid currents.

$$i_{sRq} = W_{Fq}u_{Rq},\ i_{sYq} = W_{Fq}u_{Yq},\ i_{sBq} = W_{Fq}u_{Bq} \quad (27)$$

The following method is used to calculate three-phase reference grid currents.
Grid flows, as well as the error in each phase, are used to generate the pulses for each VSC leg using the retro PWM controller.

IV. NEW PROPOSED CONTROL ALGORHTM

A.Calculation of active component of load current

"Load active power" is created through the use of the delta-bar-delta NN technique to represent current and load voltages, which have been combined to create dirty load current. The input layer here is described as

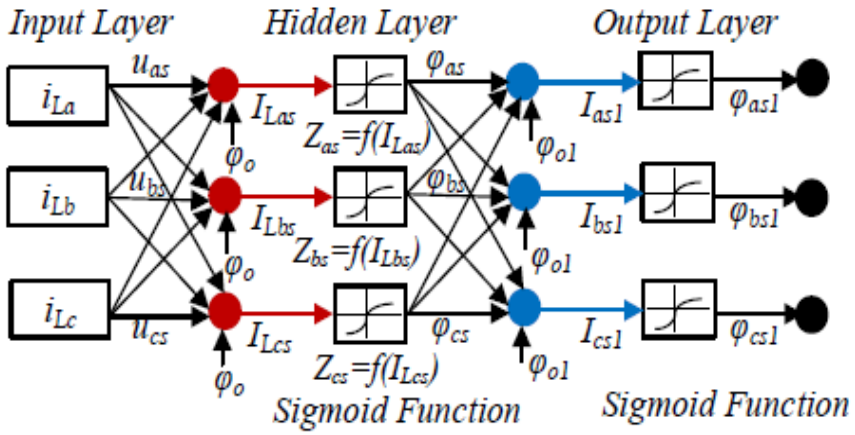

Figure 2. Proposed model of Delta-Bar-Delta NN based extraction of weighted fundamental load active power components.

$$\begin{bmatrix} I_{as} \\ I_{bs} \\ I_{cs} \end{bmatrix} = \begin{bmatrix} \varphi_a \\ \varphi_b \\ \varphi_c \end{bmatrix} + \begin{bmatrix} u_{ac} & u_{bc} & u_{cc} \\ u_{ac} & u_{cc} & u_{cc} \\ u_{cc} & u_{cc} & u_{bc} \end{bmatrix} \begin{bmatrix} i_{ca} & i_{cb} & i_{cc} \\ i_{cb} & i_{cc} & i_{cb} \\ i_{cc} & i_{cc} & i_{cb} \end{bmatrix} \quad (28)$$

Uas, Ubs, Ucs are the unit templates in phase with the POI phase voltage, and o is a bias weight.

B. Implementation of Delta-Bar-Delta Learning Technique

It is determined by averaging line condition power factor value of the load, and then multiplying it by the weight of the load (Lsa). Phase 'a' in this instance will have a modified weight equal to the weight of phase 'a' plus the weight of phase 'b'.

$$\Delta\varphi(p) = \xi\Delta\varphi(p-1) - (1-\xi)\varepsilon_p f'(I_{as1}) Z_{as}(p) \quad (29)$$

In other words, the source current gradient derivative (dp) is calculated for each sampling instant (pth). in terms of delta-bar-delta error reduction, the error that has to be decreased is computed as.

$$E_a(p) = i_{La}(p) - u_{as}(p)\varphi_{as1}(p) \quad (30)$$

In simpler terms, the exponential average of past error derivatives is known as Fp. To show how an error is going down, it specifies in which direction.

$$\varphi_{as1} = f(I_{as1}) = 1/(1+e^{-I_{as1}}) \quad (31)$$

The average exponentially differing derivative returns has a weighted of 1. In other words, the weightings decide whether long-term or present trends have a larger effect on forecasting precision. When using the delta bar delta method, there are only small modifications when dpfp is negative and larger adjustments if dpfp has a positive value.

$$\varepsilon_p = \begin{cases} \varepsilon_{p-1} + \kappa \; for \; d_p f_p > 0 \\ \varepsilon_{p-1} \times \phi \; for \; d_p f_p \le 0 \end{cases} \quad (32)$$

The present weight change is observed when a major learning rate, p, is selected (p). In order to adjust the weights in an adaptive way, we use the momentum-based objective function while doing delta-bar delta learning. Projecting the average of past weight swings helps to minimize the net weight gain from online weight training. When phase 'a' is altered, its weight is represented as follows. Also, the value at sampling instant p (Lsa(p)) is the weighted average value of the active and reactive components, whereas the phase 'a' weighted value (as(p)) is the corresponding component at that instant. The product Z(p) and the input a(p) are the results of the absorption column. The derivative of the Ias1 component, f'(Ias1), is shown by f' (Ias1). Because of this, numbers such as 0.1, 0.5, and recently 0.7 are often utilized for various kinds of difficulties and problems. When one tries to optimize, the momentum term takes into account the previous weight's effect on the present weight gain. To determine a new weight increase, it is calculated by taking the current gradient and prior weight change into consideration. The momentum and prior history do not apply if the net force is zero. If the current change is completely reliant on the prior change, then it will not affect the future. It is also true that when the values of fall between zero and one, the

combined response to changes in weight occurs. Otherwise, it is zero. Because of this, each weight change would have to be completely dependent on all preceding weight changes, and all previous weight changes would go all the way back to the original weight change, demonstrating that all weight changes are recursive. The current weight shift decreases oscillations and accuracy because the velocity raises the current weight shift. For example, in the case of sudden utility grid conditions, you will want to respond quickly, and the recommended method will enable you to do so.

This means that for the following phases, this will be shown as follows:

$$\varphi_{as}(p)=\varphi_{Lsa}(p)+\xi\{\varphi_{Lsa}(p)-\varphi_{as1}(p)\}-(1-\xi)\varepsilon_p f'(I_{as1})Z_{as}(p) \quad (33)$$

$$\varphi_{bs}(p)=\varphi_{Lsa}(p)+\xi\{\varphi_{Lsa}(p)-\varphi_{bs1}(p-1)\}-(1-\xi)\varepsilon_p f'(I_{bs1})Z_{bs}(p) \quad (34)$$

$$\varphi_{cs}(p)=\varphi_{Lsa}(p)+\xi\{\varphi_{Lsa}(p)-\varphi_{cs1}(p-1)\}-(1-\xi)\varepsilon_p f'(I_{cs1})Z_{cs}(p) \quad (35)$$

Using the Ias1, Ibs1, and Ics1 values, the active fundamental component is calculated in the sigmoid function.

$$\varphi_{as1}=f(I_{as1})=1/(1+e^{-I_{as1}}) \quad (36)$$

$$\varphi_{bs1}=f(I_{bs1})=1/(1+e^{-I_{bs1}}) \quad (37)$$

$$\varphi_{cs1}=f(I_{cs1})=1/(1+e^{-I_{cs1}}) \quad (38)$$

The graph in Fig. 3 shows that the activation function multiplied with a scaling factor of k gives rise to the signal, which is between 0 and 1. whereas standard and reference ones are calculated using those methods, the basic feature of average upgrading facilities is measured using as1, bs1, cs1 (Lsa).

$$\varphi_{Lsa}=(\varphi_{as1}+\varphi_{bs1}+\varphi_{cs1})/3 \quad (39)$$

The first-order low-pass filter is used to filter out low-frequency sounds. average power of the weighted active power (Lsa).

V. SIMULATED RESULTS

A complex investigation is done to model the AL-BP power quality performance for grid interactive improved power quality solar PV-battery backed systems using delta-bar-delta algorithm-based control technique for single-phase and unbalance three-phase four-wire (3P-4W) nonlinear loads. The simulated results shown in Figures 3 and 4 were provided in a study in which delta-bar-delta neural network-based control methods were used. When feeding three different types of single phase loads, three phase current balances, equal flows, and sinusoidal oscillations of flow will occur.

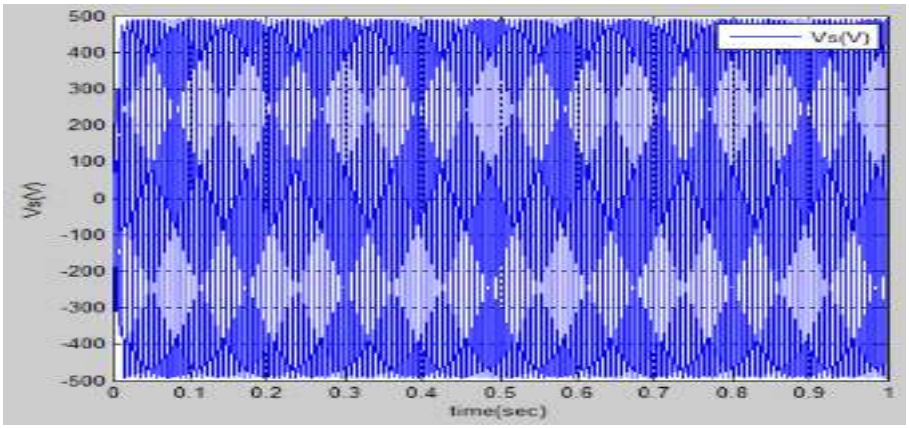
Vs(V)
Vs(V)
time(sec)

(a)

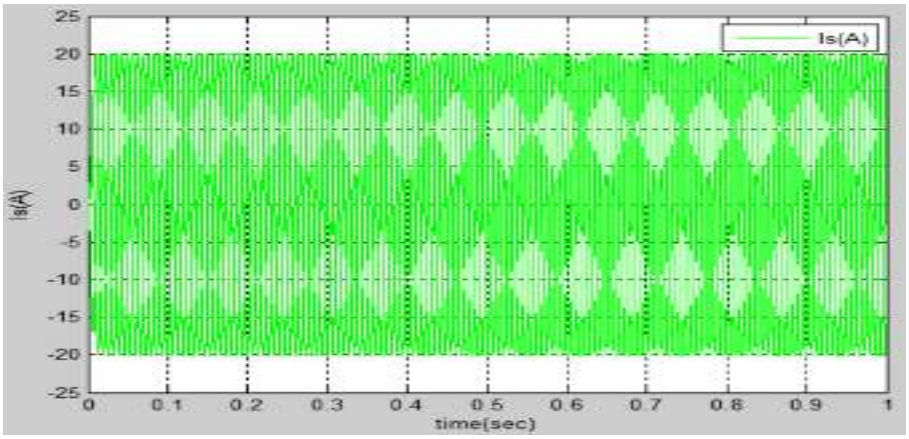
Is(A)
Is(A)
time(sec)

(b)

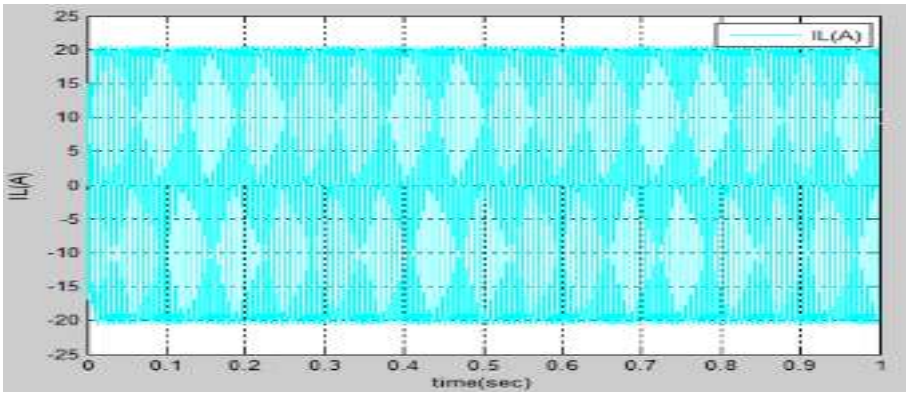
IL(A)
IL(A)
time(sec)

(c)

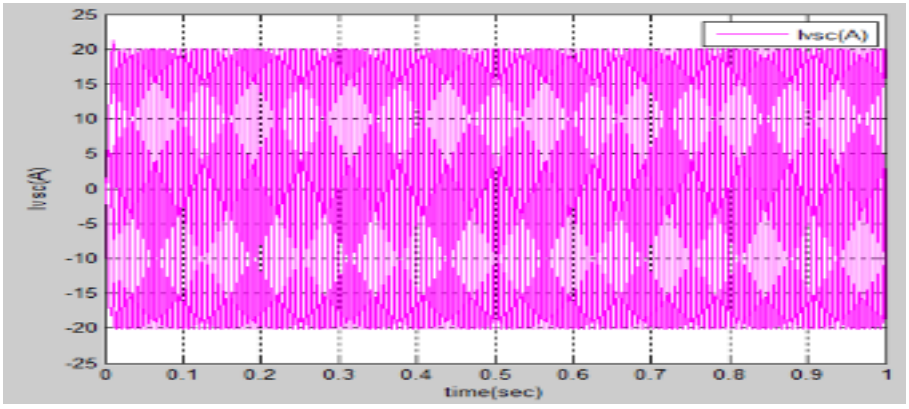
Isc(A)
Isc(A)
time(sec)

(d)

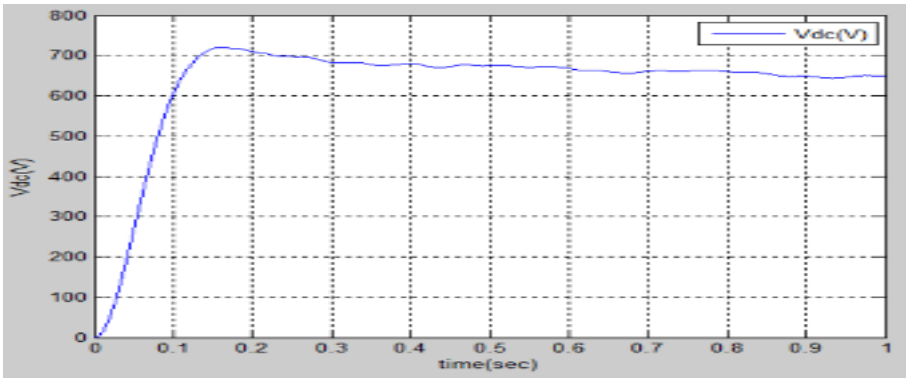

(e)

Figure 3. (a) "(a) Grid Voltages (vs), (b) Grid Currents (is), (c) Load Currents (il), (d) VSC Currents (ivsc) and (e) DC Link Voltage (VDC)"

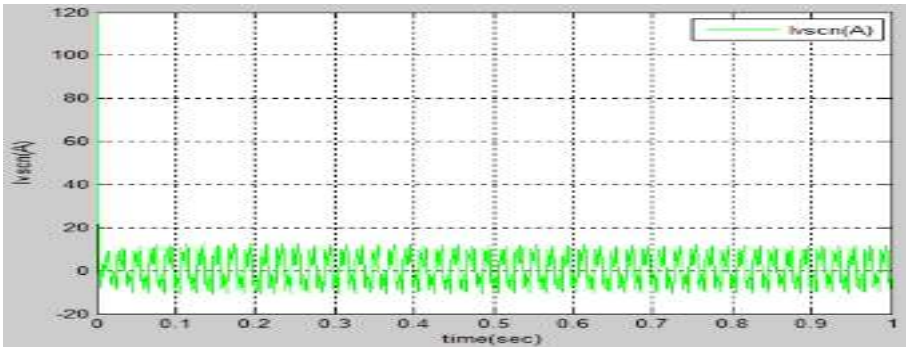

(a)

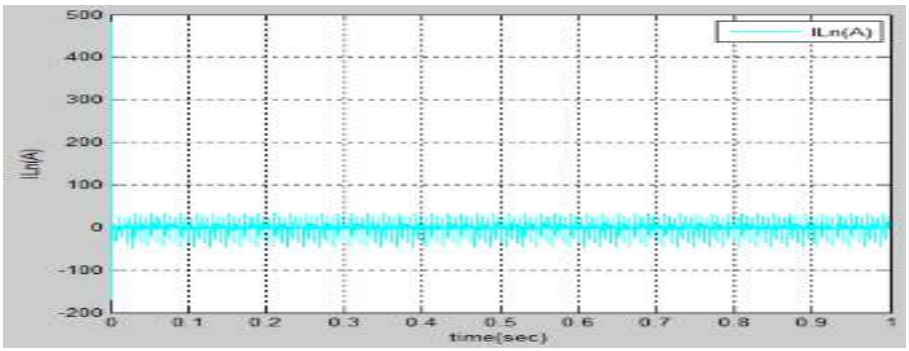

(b)

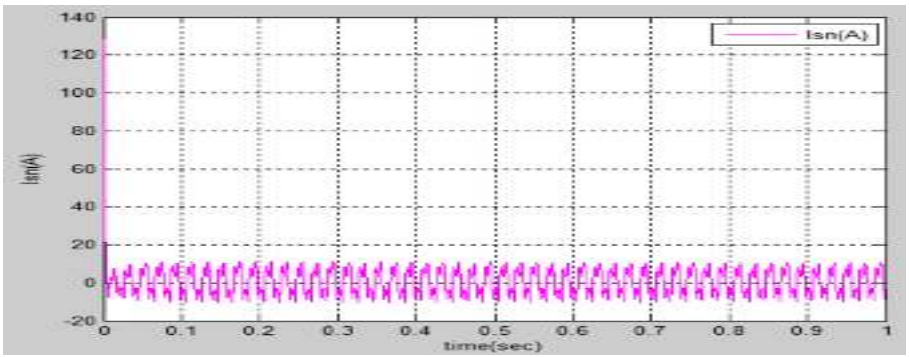

(c)

Figure 3. (b) "(a) Load Neutral Currents (iln), (b) Grid Neutral Current (isn), (c) VSC-Neutral Current (ivscn)"

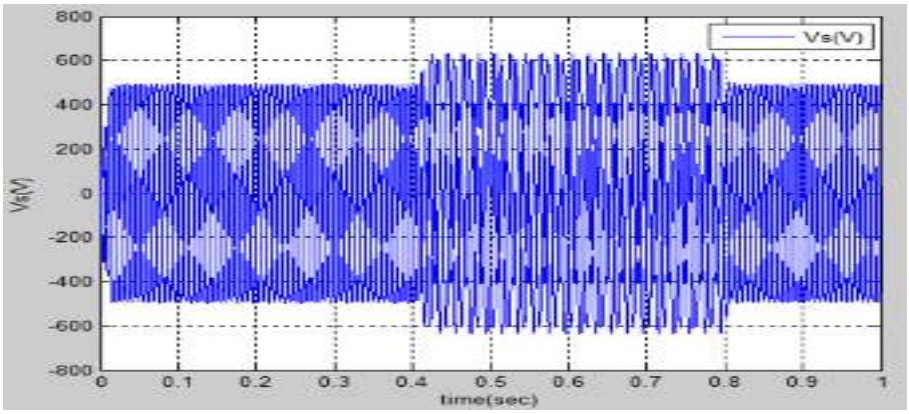

(a)

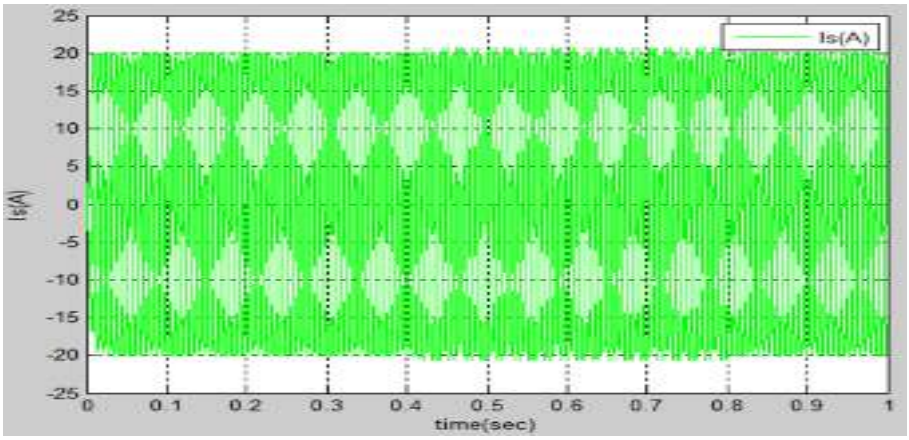

(b)

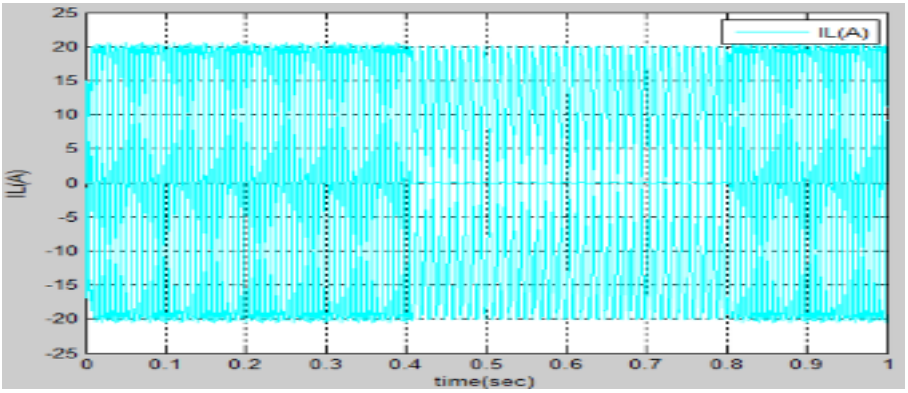

(c)

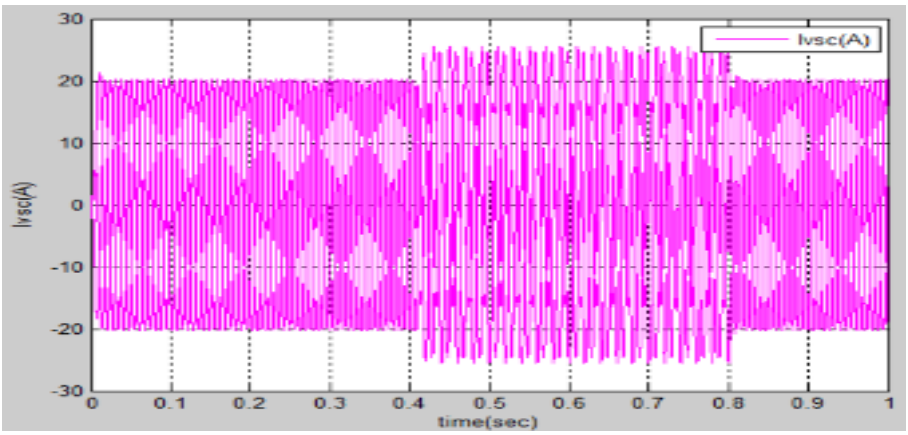

(d)

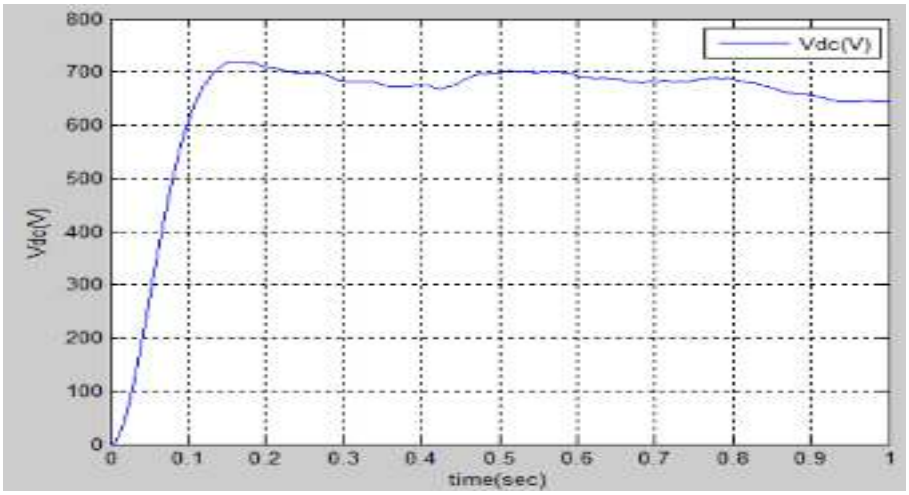

(e)

Figure 4. (a) "(a) Grid Voltages (vs), (b) Grid Currents (is), (c) Load Currents (il), (d) VSC Currents (ivsc) and (e) DC Link Voltage (VDC)"

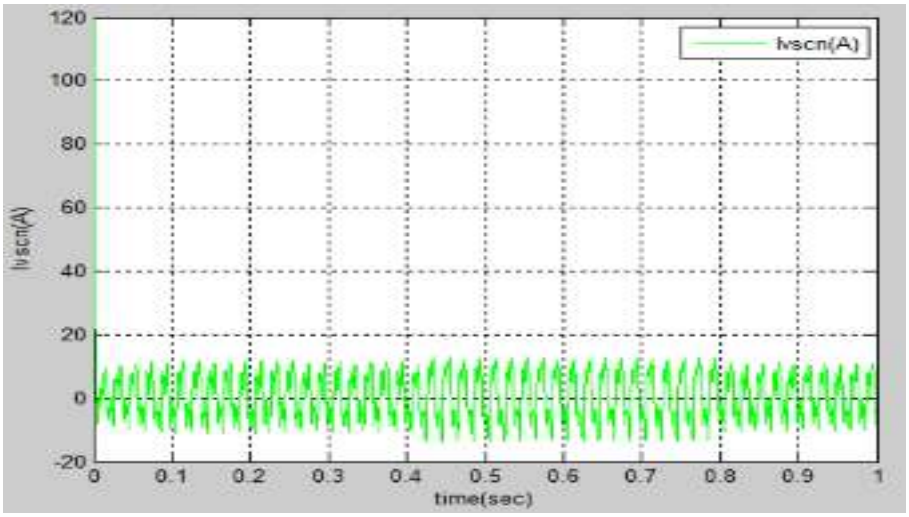

(a)

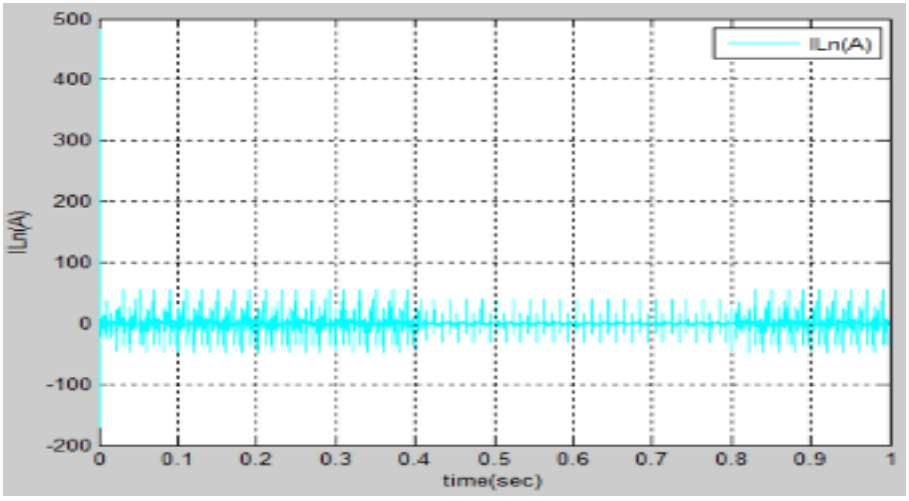

(b)

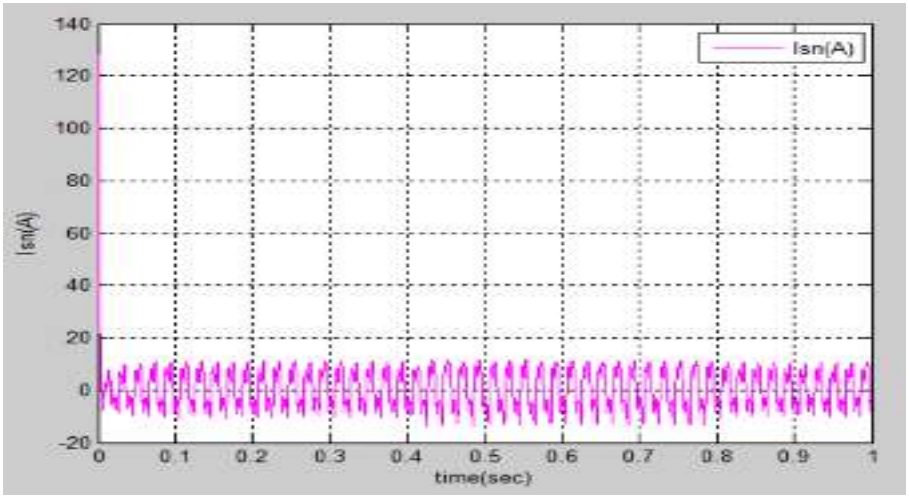

(c)

Figure 4. (b) "(a) Grid Voltages (vs), (b) Grid Currents (is), (c) Load Currents (il), (d) VSC Currents (ivsc) and (e) DC Link Voltage (VDC)"

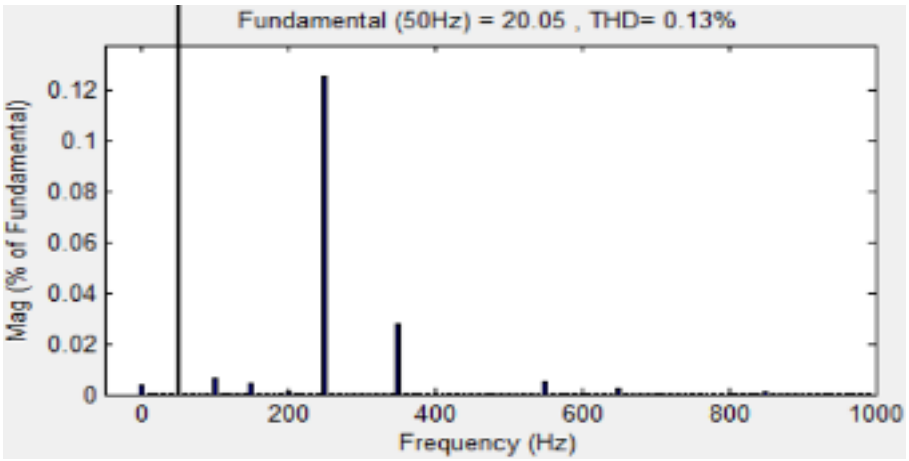

Figure 5. Harmonic spectrum of the grid current in Phase R (IsR)

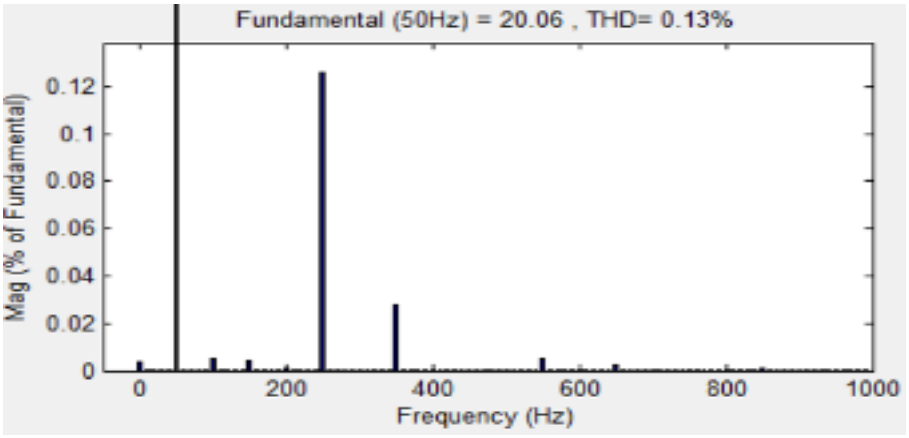

Figure 6. Harmonic spectrum of the grid current in Phase Y (IsY)

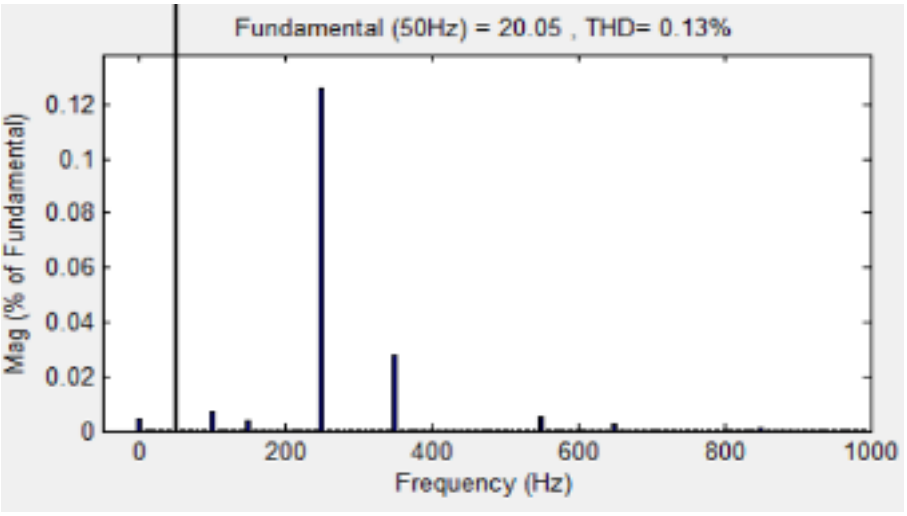

Figure 7. Harmonic spectrum of the grid current in Phase B (IsB)

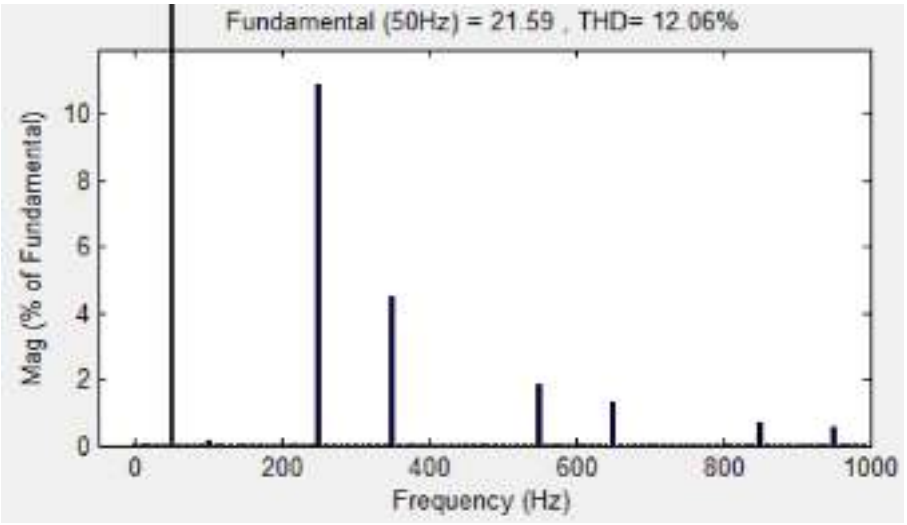

Figure 8. Harmonic spectrum of the Load current in Phase R (ILR)

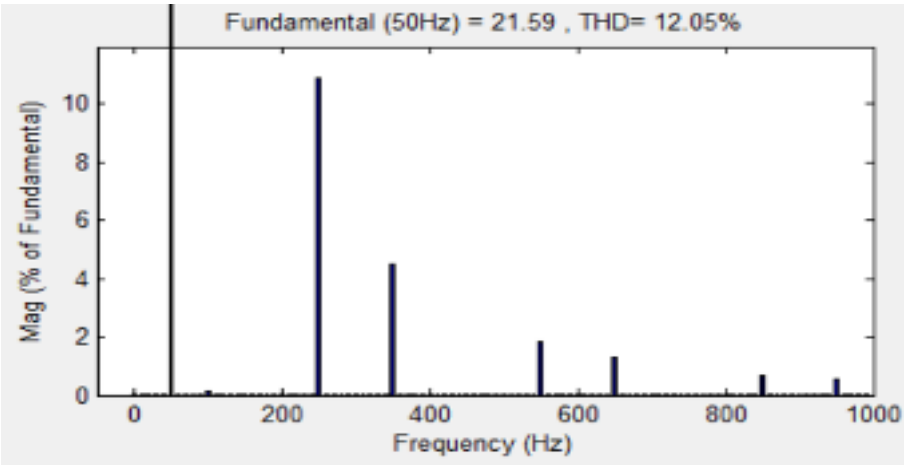

Figure 9. Harmonic spectrum of the Load current in Phase Y (ILY)

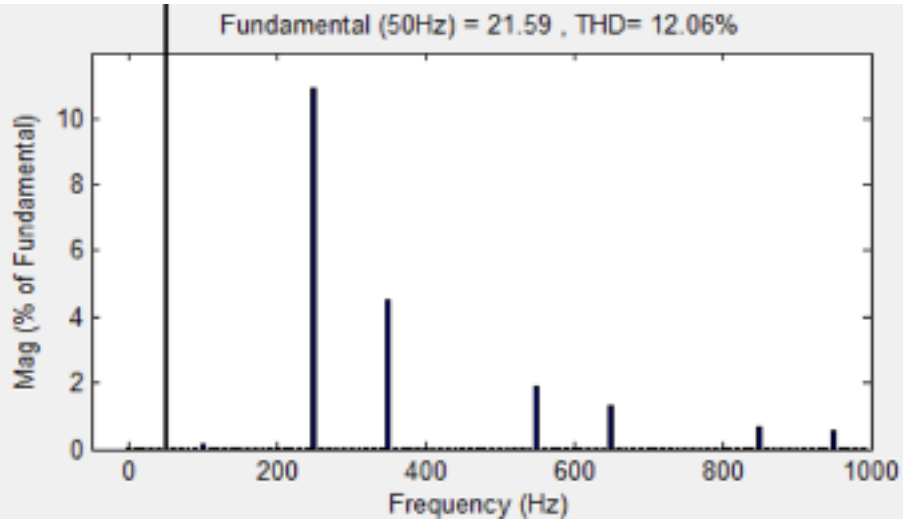

Figure 10. Harmonic spectrum of the Load current in Phase B (ILB)

The simulated results show that the load's neutral current has been perfectly balanced by fourth leg of the VSC. To achieve zero harmonics of load-neutral current, a neutral's current must be kept equal to zero. to maintain equal and balanced three-phase currents at the grid's side, the shape of current of VSC is changed The waveforms and THDs of the grid currents are illustrated in figure 5a. As you can see in Figure 5(b), the load current waveforms and THDs are shown. estimate in Figure 5(a) shows that THD in grid current is less than 1% (b). It is permitted since this system is in full compliance with the IEEE 519 standard. It shows the system's performance when severely unbalanced in Figure 4. The other two phases are giving power to a 1-phase linear and nonlinear system, while the first phase is powering just the system. a balanced 3-phase and single-phase nonlinear and linear load arrangement was seen in the steady state simulation of the integrated 3-phase 4 wire grid solar PV/battery system with steady state simulation shown in Illustration 3A-3 (b). This result shows that all three phases of the grid-side current are equal and sinusoidal, with equal but uneven amounts of loading. The grid supplies a non-sinusoidal current of roughly triangular shape, which is fully rectified by the fourth leg of VSC. By measuring the THD (Toward Harmonic Distortion) of a single-phase nonlinear load in comparison to grid current, it was found that the THD of the current being fed into the system is 32.83% compared to 5%, which shows that the system is in conformity with IEEE Standard 519.

VI. CONCLUSİON

Performance of the system and energy quality were greatly improved due to grid interaction. In this article, the authors propose a solar-PV-battery-assisted system using the delta-bar-delta neural network-based control technique. MPPT (Maximum Power Point Tracking) was used to optimize the power output of the solar power array. Many of the techniques carried out by the control method serve many functions. One of them is managing the load and its harmonics. Several grid conditions have proven the grid-tied PV system to be dependable, including voltage sag, instability in the load, and reduced solar insolation. Another thing that

was found is that regardless of operating and loading conditions, such as when there is an imbalance load on one of the phases, the supply currents are even and sinusoidal. The proposed system meets the IEEE power quality standard.

REFERENCES

[1] *Basic* F. -. Chen, "Back-propagation neural networks for nonlinear self-tuning adaptive control," *IEEE Control Systems Magazine*, vol. 10, no. 3, pp. 44-48, April 1990.

[2] S. Siu, Ching-Haur Chang and Che-Ho Wei, "L/sub p/ norm back propagation algorithm for adaptive equalization," *IEEE Transactions on Circuits and Systems II: Analog and Digital Signal Processing*, vol. 42, no. 9, pp. 604-607, Sept. 1995.

[3] C. -. Hsu, M. -. Kang and C. -. Chen, "Design of adaptive load shedding by artificial neural networks," *IEE Proceedings - Generation, Transmission and Distribution*, vol. 152, no. 3, pp. 415-421, 6 May 2005

[4] Hsi-Chin Hsin, Ching-Chung Li, Mingui Sun and R. J. Sclabassi, "An adaptive training algorithm for back-propagation neural networks," *IEEE Transactions on Systems, Man, and Cybernetics*, vol. 25, no. 3, pp. 512-514, March 1995.

[5] P. Zhao and O. P. Malik, "Design of an Adaptive PSS Based on Recurrent Adaptive Control Theory," *IEEE Transactions on Energy Conversion*, vol. 24, no. 4, pp. 884-892, Dec. 2009.

[6] P. Wei, C. Cheng and T. Liu, "A Photonic Transducer-Based Optical Current Sensor Using Back-Propagation Neural Network," *IEEE Photonics Technology Letters*, vol. 28, no. 14, pp. 1513-1516, 15 July15, 2016.

[7] L. Jin, P. N. Nikiforuk and M. M. Gupta, "Direct adaptive output tracking control using multilayered neural networks," *IEE Proceedings D - Control Theory and Applications*, vol. 140, no. 6, pp. 393-398, Nov. 1993.

[8] T. Jain, S. N. Singh and S. C. Srivastava, "Adaptive wavelet neural network-based fast dynamic available transfer capability determination," *IET Generation, Transmission & Distribution*, vol. 4, no. 4, pp. 519-529, April 2010.

[9] M. Saerens and A. Soquet, "Neural controller based on back-propagation algorithm," *IEE Proceedings F - Radar and Signal Processing*, vol. 138, no. 1, pp. 55-62, Feb. 1991.

[10] S. Cong and Y. Liang, "PID-Like Neural Network Nonlinear Adaptive Control for Uncertain Multivariable Motion Control Systems," *IEEE Transactions on Industrial Electronics*, vol. 56, no. 10, pp. 3872-3879, Oct. 2009.

[11] R. C. Frye, E. A. Rietman and C. C. Wong, "Back-propagation learning and nonidealities in analog neural network hardware," *IEEE Transactions on Neural Networks*, vol. 2, no. 1, pp. 110-117, Jan. 1991.

[12] W. Ding and D. Liang, "Modeling of a 6/4 Switched Reluctance Motor Using Adaptive Neural Fuzzy Inference System," *IEEE Transactions on Magnetics*, vol. 44, no. 7, pp. 1796-1804, July 2008.

[13] P. J. Antsaklis, "Neural networks for control systems," *IEEE Transactions on Neural Networks*, vol. 1, no. 2, pp. 242-244, June 1990.

[14] F. D. Zahlay, K. S. Rama Rao and T. B. Ibrahim, "A New Intelligent Autoreclosing Scheme Using Artificial Neural Network and Taguchi's Methodology," *IEEE Transactions on Industry Applications*, vol. 47, no. 1, pp. 306-313, Jan.-Feb. 2011.

[15] P. Shamsollahi and O. P. Malik, "Direct neural adaptive control applied to synchronous generator," *IEEE Transactions on Energy Conversion*, vol. 14, no. 4, pp. 1341-1346, Dec. 1999.

[16] J. Sztipanovits, "Dynamic backpropagation algorithm for neural network controlled resonator-bank architecture," *IEEE Transactions on Circuits and Systems II: Analog and Digital Signal Processing*, vol. 39, no. 2, pp. 99-108, Feb. 1992.

[17] Li-Min Du, Zi-QiangHou and Qi-Hu Li, "Optimum block-adaptive learning algorithm for error back-propagation networks," *IEEE Transactions on Signal Processing*, vol. 40, no. 12, pp. 3032-3042, Dec. 1992.

[18] M. Aredes and E. H. Watanabe, "New control algorithms for series and shunt three-phase four-wire active power filters," *IEEE Transactions on Power Delivery*, vol. 10, no. 3, pp. 1649-1656, 1995.

[19] M. J. Ryan, R. W. De Doncker and R. D. Lorenz, "Decoupled control of a four-leg inverter via a new 4×4 transformation matrix," *IEEE Transactions on Power Electronics*, vol. 16, no. 5, pp. 694-701, 2001.

[20] R. R. Sawant and M. C. Chandorkar, "A Multifunctional Four-Leg Grid-Connected Compensator," *IEEE Transactions on Industry Applications*, vol. 45, no. 1, pp. 249-259,2009.

[21] Z. Zeng, H. Yang, J. M. Guerrero and R. Zhao, "Multi-functional distributed generation unit for power quality enhancement," *IET Power Electronics*, vol. 8, no. 3, pp. 467-476,2015.

[22] A. K. Panda and R. Patel, "Adaptive hysteresis and fuzzy logic controlled-based shunt active power filter resistant to shoot-through phenomenon," *IET Power Electronics*, vol.8,no.10,pp.1963-1977,2015.

[23] Y. Karimi, J. M. Guerrero and H. Oraee, "Decentralized method for load sharing and power management in a hybrid single/three-phase islanded microgrid consisting of hybrid source PV/battery units," *2016 IEEE Energy Conversion Congress and Exposition (ECCE)*, Milwaukee, WI,pp.1-8,2016.

[24] Y. Karimi, J. M. Guerrero and H. Oraee, "Decentralized method for load sharing and power management in a hybrid single/three-phase islanded microgrid consisting of hybrid source PV/battery units," *2016 IEEE Energy Conversion Congress and Exposition (ECCE)*, Milwaukee,WI,pp.1-8, 2016.

[25] A. Merabet, K. Tawfique Ahmed, H. Ibrahim, R. Beguenane and A. M. Y. M. Ghias, "Energy Management and Control System for Laboratory Scale Microgrid Based Wind-PV-Battery," *IEEE Transactions on Sustainable Energy*, vol. 8, no. 1, pp. 145-154, 2017.

[26] M. O. Badawy and Y. Sozer, "Power Flow Management of a Grid Tied PV-Battery System for Electric Vehicles Charging," in *IEEE Transactions on Industry Applications*, vol.53,no.2,pp.1347-1357,2017.

[27] A. Mohd *et al*., "Control strategy and space vector modulation for three-leg four-wire voltage source inverters under unbalanced load conditions," in *IET Power Electronics*, vol. 3, no. 3, pp. 323-333, 2010.

[28] Ujjwal Kumar Kalla and Madhuri Mantri, " An Adaptive Control of Voltage Source Converter Based Scheme for Grid connected Solar PV-Battery System," in proc. of *Seventh IEEE Power India International Conference 2016*, pp. 1-6.

[29] B. Singh and S. R. Arya, "Back-Propagation Control Algorithm for Power Quality Improvement Using DSTATCOM," *IEEE Transactions on Industrial Electronics*, vol. 61, no. 3, pp. 1204-1212, March 2014.

[30] B. Subudhi and R. Pradhan, "A comparative study on maximum power point tracking techniques for photovoltaic power systems," *IEEE Trans. on Sustainable Energy*, vol. 4, no. 1, pp. 89-98, , January 2013.

[31] M. Jazayeri, S. Uysal, and K. Jazayeri, "Evaluation of maximum power point tracking techniques in PV systems using MATLAB/Simulink," *Sixth Annual IEEE Green Technologies Conf.*, 2014, pp. 54-60.